JOURNAL OF MATERIALS SCIENCE 27 (1992) 3803–3806

Relationship between ageing and deformation characteristics, and microdefects in aluminium–lithium alloys: an X-ray double crystal diffractometry study

V. GONDHALEKAR, J. CHAUDHURI, A. INCHEKEL, J. E. TALIA
Mechanical Engineering Department, National Institute for Aviation Research, The Wichita State University, Wichita, KS 67208, USA

A non-destructive X-ray technique, the double crystal diffractometer method, is presented as a tool to investigate the ageing and deformation characteristics of aluminium–lithium alloys. This method is extremely sensitive and can be used to measure strains and dislocation densities through the rocking curve half-width. X-ray data were used to correlate the different stages of the microstructure during ageing and deformation. Models were also developed to describe the microstructural behaviour of these alloys.

1. Introduction

In the recent past, the aerospace and automobile industries have recognized the growing importance of aluminium–lithium (Al–Li) alloys because of their low-density–high-strength characteristics. A useful investigation would be to study ageing and deformation characteristics in these materials.

When Al–Li alloys, containing more than 1 wt % Li, are quenched from the single-phase field and aged at a temperature below the metastable solvus line, homogeneous precipitation of a metastable phase of δ' (Al_3Li) occurs. This phase is a superlattice with a Cu_3Au (Li_2) type structure. Due to the structural similarity and close match between the lattice parameters of the solid solution and the δ' precipitate, a homogeneous distribution of coherent precipitates is observed [1, 2]. Changes in the elastic modulus and density of the alloy occur irrespective of the amount of lithium being present in the material or δ' precipitate. However, improvement in the strength is accompanied by the nucleation and growth of the precipitates.

The X-ray double crystal diffractometer (DCD) technique is an extremely sensitive method for measuring microdeformations and microdefects in materials [3–5]. This method is non-destructive, rapidly performed, and needs no sample preparation. It is well suited to the study of mechanical properties when the degree of deformation is small.

In this article precipitation hardening characteristics and deformation mechanisms of the Al–Li alloy, as characterized by the X-ray double crystal diffractometry, are reported.

2. Experiment

Kaiser 2090 Al–Li (2.6 wt % Li) alloy, with a grain size of about 15 μm, was used in the present study. Since for X-ray measurement, the minimum size of the grain required is approximately 50 μm, it was necessary to obtain a larger grain size. The strain-anneal technique was selected for this purpose. The sheet specimens were at first deformed 0.7% and annealed at 550 °C for 2 h, followed by quenching to room temperature. The larger grains (about 1000 μm) were selected for the X-ray analysis. Subsequent ageing treatment were performed at 160 °C, 200 °C, and 240 °C, respectively.

After each ageing treatment, the Vickers microhardness of the specimen was measured by using a Leco microhardness apparatus. Also, the X-ray analysis was performed in a different area of the specimen by using a Blake industries double crystal diffractometer in (+ −) parallel arrangement and the CuK_α radiation. The beam size of the X-ray used was 0.5 mm by 0.5 mm. A crystal of germanium (1 1 1 surface) was used as the first crystal and X-ray rocking curves of the (0 0 2) reflection were obtained from individual grains of the Al–Li alloy. The details of the X-ray rocking curve analysis technique and its application to polycrystalline materials is described elsewhere [4, 5]. Both the peak intensity (PI) and full width at half-maximum (FWHM) are measures of lattice misalignment caused by strains and/or dislocations. As lattice misalignment increases, PI decreases and FWHM increases.

In the deformation work, 1.27 mm square grids were first electrochemically etched on the specimen surface. The specimens were pulled in tension in an MTS machine. The deformation was accomplished in steps of 0.8% until failure. Each grid was measured and recorded after each stage of deformation to obtain the strains parallel and perpendicular to the tensile direction; also X-ray analysis was performed after each deformation. The CuK_α radiation with an X-ray beam size of 1 mm by 1 mm was used to obtain

0022–2461

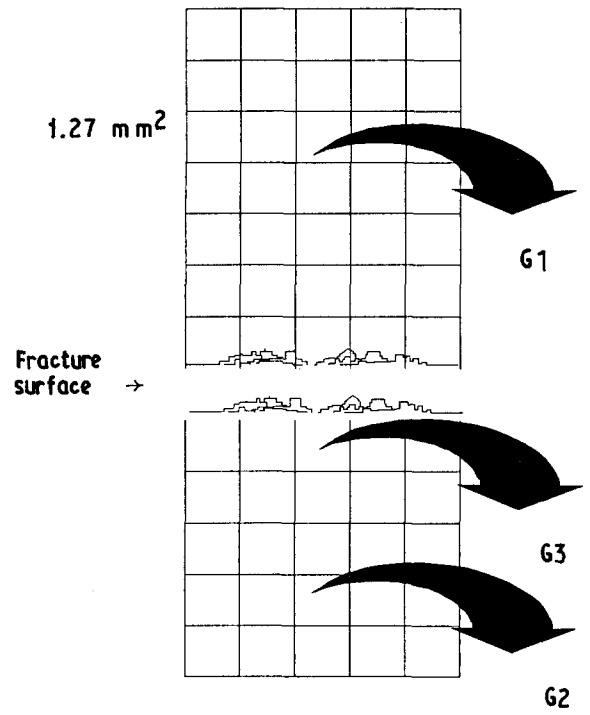

Figure 1 Schematic diagram showing the position of the grids, with respect to the fracture surface, in which X-ray rocking curve measurements were performed.

rocking curves of the (0 0 2) reflection from individual grids in the sample as shown in Fig. 1. Both the FWHM and PI were obtained from the rocking curve.

3. Results and discussions

The variation of microhardness with ageing time for three different ageing temperatures (160, 200 and 240 °C) are shown in Fig. 2. The strength or hardness associated with the precipitates is due to their resistance to dislocation motion. Details of the strengthening mechanism in two-phase alloys by the second-phase particles can be obtained elsewhere [6]. For shearable precipitates such as Al_3Li this depends mainly on coherency hardening, which is the elastic coherency stress surrounding a particle that does not fit into the matrix exactly. It can be seen in Fig. 2 that the maximum hardness was obtained at 8 h ageing at 240 °C, and at 32 h ageing at 160 °C and 200 °C, since maximum coherency occurred at these times respectively. Ageing longer than 8 h at 240 °C, and 32 h at 160 °C and 200 °C led to coarsening of the precipitates, which was accompanied by gradual loss of coherency and hence decrease in hardness. In addition, it is noticeable in Fig. 2 that the optimum temperature for maximum hardness of this alloy is 200 °C.

The ratios of the FWHM to maximum FWHM and the peak intensity to the maximum peak intensity, as averaged over a number of grains are plotted against ageing time in Figs 3 and 4, respectively. At the beginning, the FWHM decreases and the peak intensity increases probably due to the release of internal stresses generated during quenching, and/or more volume fraction of the matrix was getting aligned and satisfying the Bragg diffraction condition as the precipitate particles were leaving the matrix. Subsequent increase in FWHM and decrease in PI values were due to the increasing lattice misalignment caused by the increase in coherency strains with the growth of precipitate particles. Beyond the optimum ageing time at each ageing temperature, the FWHM should decrease and PI should increase due to the reduction in coherency strains. On the contrary, the FWHM increased and PI decreased, which indicated that dislocation multiplication occurred for ageing beyond

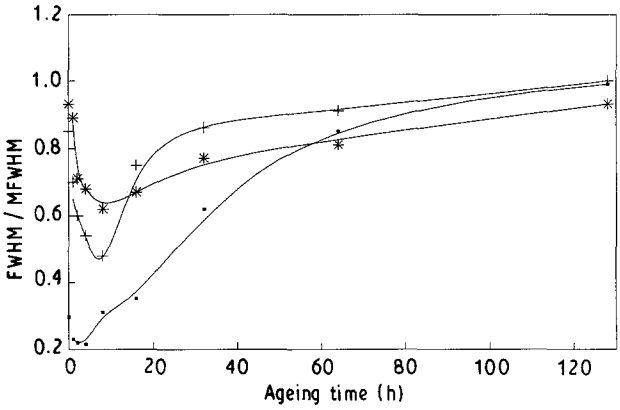

Figure 3 Variation of the FWHM/maximum FWHM with the ageing time at three different temperatures: (⊡) 200 °C, (+) 240 °C, (*) 160 °C.

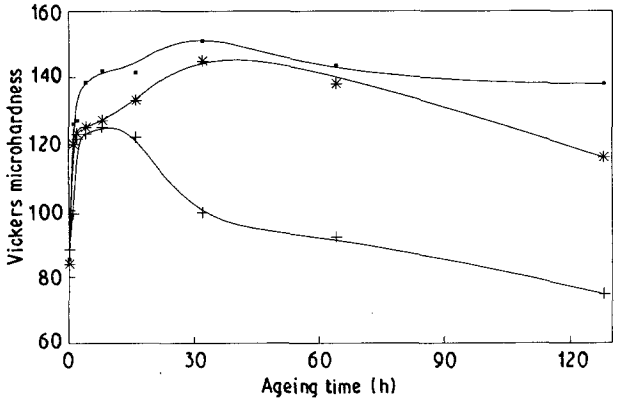

Figure 2 Variation of the microhardness of the 2090 Al–Li alloy with the ageing time at three different temperatures: (⊡) 200 °C, (+) 240 °C, (*) 160 °C.

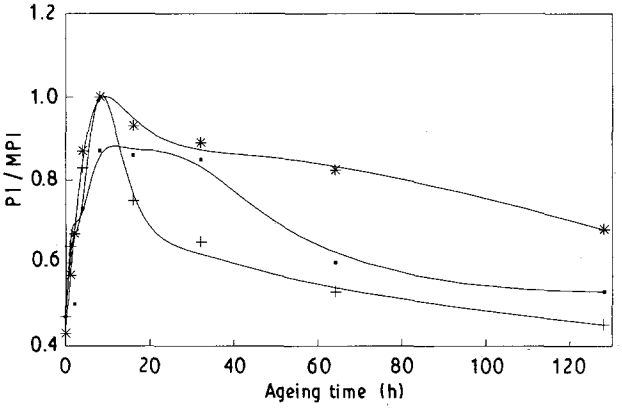

Figure 4 Variation of the peak intensity/maximum peak intensity with the ageing time at three different temperatures: (⊡) 200 °C, (+) 240 °C, (*) 160 °C.

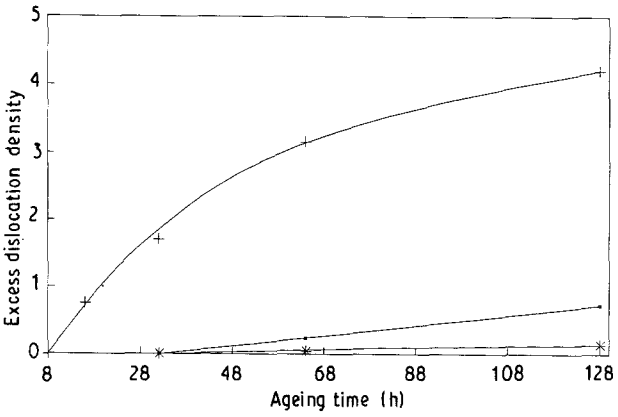

Figure 5 Excess dislocation density, compared with the dislocation density at optimum ageing time, plotted against time for three different ageing temperatures: (⊡) 200 °C, (+) 240 °C, (*) 160 °C.

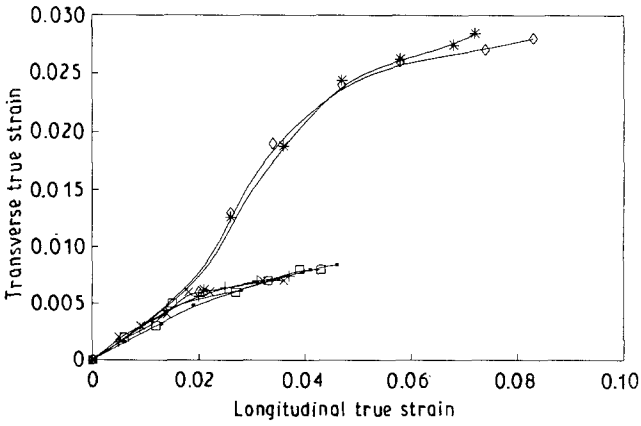

Figure 7 Transverse true strain plotted against longitudinal true strain for three different grids. Sample 1: (–■–) G1, (+) G2, (*) G3; sample 2: (–⊟–) G1, (–×–) G2, (–◇–) G3.

the optimum time at each temperature. Moreover, smaller slopes at longer ageing time in the microhardness, FWHM and PI curves can be attributed to the strengthening mechanism due to entanglement of dislocations. The excess dislocation densities beyond the optimum ageing time at each ageing temperature are plotted in Fig. 5. The dislocation density, D, is calculated from the FWHM as $D = (\text{FWHM})^2/9b^2$, where b is the Burgers vector.

Fig. 6 shows the magnitude of the longitudinal true strain in different grids at each stage of deformation in one of the samples. Grid number zero represents the fractured grid. The plot clearly shows that the strain in the fractured grid at every stage of deformation is higher than in the other grids as expected. The maximum true strain is 8% at the fracture grid and 4% at grids away from the fracture surface. Fig. 7 shows a plot of the transverse true strain versus the longitudinal true strain for the two samples. It is seen here that up to 4% deformation the pattern is same for all grids and then the fractured grid breaks away indicating a change in mode of deformation.

Fig. 8 shows the ratio of the PI to the maximum PI for different grids in two different samples. It can be clearly seen that there is much more decrease in the peak intensity ratio with the increase in deformation

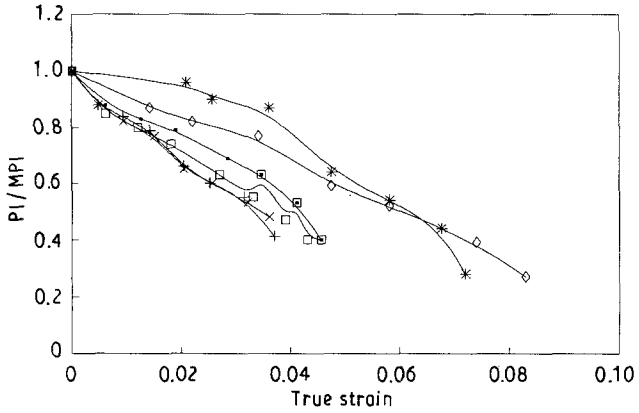

Figure 8 Peak intensity/maximum peak intensity plotted against true strain for three different grids. Sample 1: (–■–) G1, (+) G2, (*) G3; sample 2: (–⊟–) G1, (–×–) G2, (–◇–) G3.

for the fractured grids than the grids away from the fractured surface.

Fig. 9 shows the ratio of the FWHM to the maximum FWHM for various grids. Here, also, it can be seen that as the deformation increases, i.e. in effect the true strain increases, the ratio of the FWHM to the maximum FWHM increases and this increase is much more for the fractured grids in the two samples.

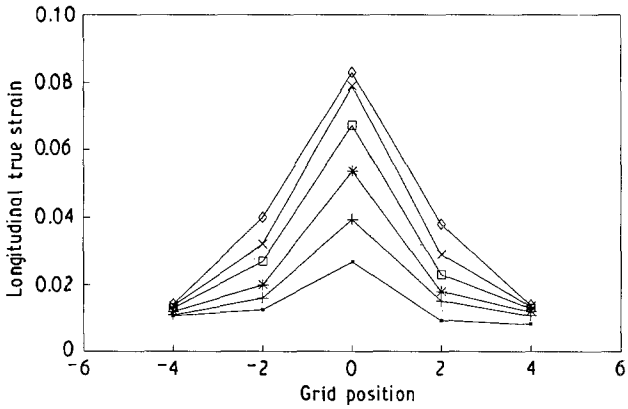

Figure 6 Longitudinal true strain plotted against grid position at different stages of deformation: (–■–) no. 2, (+) no. 3, (*) no. 4, (–⊟–) no. 5, (–×–) no. 6, (–◇–) no. 7.

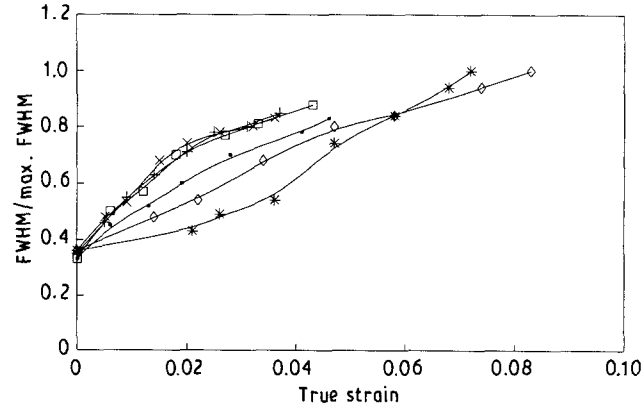

Figure 9 FWHM/maximum FWHM plotted against true strain for three different grids. Sample 1: (–■–) G1, (+) G2, (*) G3; sample 2: (–⊟–) G1, (–×–) G2, (–◇–) G3.

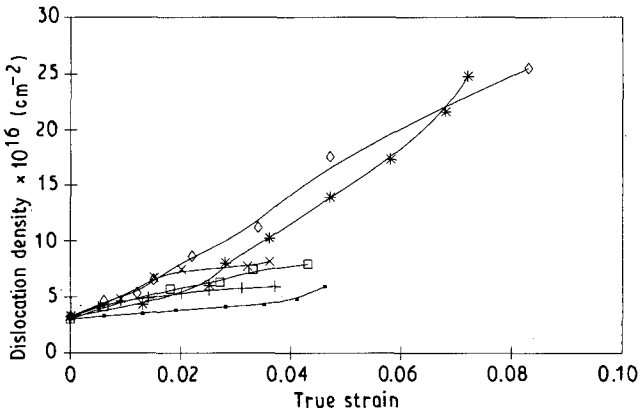

Figure 10 Dislocation density plotted against true strain for three different grids. Sample 1: (–■–) G1, (+) G2, (*) G3; sample 2: (–□–) G1, (–×–) G2, (–◇–) G3.

The dislocation density is plotted against the true strain in Fig. 10, which shows that the dislocation density increases with the increase in true strain in all grids and again dislocation multiplication is much more in the fracture grids than in the grids away from the fracture surface. The critical dislocation density, needed for fracture for both the samples, was about 25×10^{16}, and an average 4% of deformation was needed.

4. Conclusions

The X-ray double crystal diffractometry technique was utilized to follow the ageing and deformation characteristics of the aluminium–lithium alloy. This non-destructive method is an extremely sensitive way to measure the strain and dislocation density through X-ray rocking curves. The ageing experiments were performed at 160 °C, 200 °C and 240 °C, respectively. X-ray rocking curve data were used to correlate different stages of microstructure. Models were developed to describe the ageing behaviour of the alloy. For maximum hardness, the optimum ageing needed for the 2090 Al–Li alloy was found to be 32 h and the optimum temperature was 200 °C. Dislocation multiplication occurred beyond that time and reduction in hardness slowed down after 64 h of ageing. Similar behaviour was observed at other two ageing temperatures although the maximum hardness obtained was lower than that at 200 °C.

For the deformation experiment, square grids were electrochemically etched on the specimens, which were tested under tension. The FWHM and PI values within individual grids were obtained at each stage of deformation. The dislocation density versus deformation curves were plotted from which the critical dislocation density needed for fracture was obtained.

The material did not exhibit localized necking but diffused necking when pulled under tension, which is confirmed by the lower dislocation density in grids other than the fractured grids. The peak intensity ratio decreased and the FWHM increased with the increasing deformation, the decrease in PI and the increase in FWHM being more in the fractured grid indicating more lattice misalignment due to increase in dislocations in that grid. The critical dislocation density for fracture was found to be about 25×10^{16} and an average deformation of 4% was needed.

Acknowledgement

The authors gratefully acknowledge the support of this reasearch by the US Army Research Office, contract number DAAL 03-87-G-003 and the National Institute for Aviation Research at the Wichita State University.

References

1. E. A. STARKE Jr, T. H. SANDERS and I. G. PALMER, *J. Metals* **33** (1981) 24.
2. B. NOBLE and G. E. THOMPSON, *Metal Sci. J.* **5** (1971) 114.
3. B. K. TANNER, "X-ray diffraction topography" (Pergamon, 1976) p. 47.
4. R. N. PANGBORN, S. WEISSMANN and I. R. KRAMER, *Metall. Trans.* **12A** (1981) 109.
5. J. CHAUDHURI, V. GONDHALEKAR, A. INCHEKEL and J. E. TALIA, *J. Mater. Sci.* **25** (1990) 3938.
6. P. M. KELLY, *Int. Metall. Rev.* **18** (1973) 31.

Received 19 March
and accepted 1 July 1991